Resilient control design of networked vehicle suspension system under False Data Injection Attacks

Yuhui Zhang*

School of Automation, Jiangsu University of Science and Technology, Zhenjiang, China, 212100

*Corresponding author: zyh3121zj@163.com

Abstract. Under covert false data injection (FDI) attacks, the robust security control problem of nonlinear active vehicle suspension systems (AVSSs) is examined in this paper. First, the network fuzzy control active suspension model is developed, and the Takagi-Sugeno (T-S) fuzzy technology is applied to address the uncertainty of AVSSs. Secondly, considering the influence of the FDI attack model, a resilient controller is designed for AVSSs. The exponential stability condition of the system under the network assault is then derived concurrently with the design of the Lyapunov function associated with the membership degree. Lastly, a simulation test confirms the developed controller's efficacy.

Keywords: Active vehicle suspension system, resilient controller, FDI attack model, Lyapunov function.

1. Introduction

The suspension system is a crucial component of the vehicle's structure [1]. It can lessen vibration between the body and wheels and stabilize the vehicle's body. Although passive suspension does a better job of improving ride quality, it has trouble maintaining handling and road-holding capacity simultaneously. At present, several types of suspension systems have been developed, including semi-active suspension [2], active seat suspension [3], and active suspension [4] to improve the overall performance of the vehicle. Recently, extensive attention has been paid to the advantages provided by the active suspension system in achieving a compromise between three irreconcilable performances.

To motivate a more comprehensive performance, several advanced control techniques are applied to the active suspension, such as robust $H\infty$ control, event-triggered control, backstepping control, networked control, and others. Notably, due to its remarkable resilience and effectiveness in disturbance attenuation, the $H\infty$ control technique has been heavily used in the development of the active suspension controller [5]. The issue of finite frequency fuzzy $H\infty$ control for uncertain active car suspension systems with sensor failures has been examined in [6], to name a few. Focusing on the tire lateral force is susceptible to saturation. Wang et al. [7] suggested a robust $H\infty$ controller to modify the vehicle's lateral motion . In order to enhance the vertical dynamic performance of suspension systems and guarantee vehicle stability, it is crucial to research a fuzzy $H\infty$ control approach appropriate for suspension systems.

However, the sprung mass and unsprung mass will vary to some degree as a result of the vehicle's shifting passenger load and the loading and unloading of cargo. Consequently, the dynamic behavior of the suspension system is often unpredictable and nonlinear [8]. It is crucial to notice that the Takagi-Sugeno (T-S) fuzzy technique can characterize the nonlinear system and demonstrate its applicability for controller construction by weighting a collection of sub-linear systems according to the defined membership function [9]. Due to the aforementioned benefits, fuzzy technology has been extensively researched, and notable advancements have been made in a number of areas, including attack detection, controller synthesis, stability analysis, and so on. To name a few, based on the multi-instantaneous fuzzy control mechanism, Shan et al. [10] studied the safety control problem of the networked interval type-2 active suspension system. In [11], a flexible control technique for a yaw moment control system was offered by the robust $H\infty$ control method based on the T-S fuzzy model. Currently, by putting on-board terminal equipment on the dashboard, the vehicle networked control

systems (NCSs) are responsible for gathering, storing, and transmitting all of the vehicle's operating circumstances, including both static and dynamic information. The networked vehicle system typically functions as a real-time scenario and realizes human-vehicle interaction over a mobile network. Despite these benefits, NCSs also present several significant difficulties, particularly with regard to data transfer. Malicious network attacks are among the frequent issues that impact the quality of data transmission and the overall control performance of NCSs throughout the network transmission process [12]. Building a secure controller is therefore essential to shielding NCSs against malevolent attacks.

This paper mainly studies the design of suspension system controllers based on the fuzzy control model. The main work of this paper is as follows: (1) A fuzzy control strategy under FDI attacks is proposed to reduce the impact of malicious network attacks and stabilize the suspension system quickly. (2) A sufficient condition for satisfying $H\infty$ performance is derived by employing a Lyapunov function, which is related to the membership degree.

This is how the remainder of the article is structured. Section II establishes the model of a quarter car's active suspension system, and Section III provides and proves the system's exponential stability condition under the fuzzy control model. Section IV is a Simulink simulation experiment, which demonstrates how effective the control mechanism is. Section V concludes the paper.

2. Preliminaries and Model Description

2.1. Active Suspension Model with Networked Fuzzy Control

Compared with previous studies, this paper establishes a class of network attack models, considering the networked control process of the suspension system. The specific framework is shown in Figure 1. Quarter-vehicle suspension has all the characteristics of vehicle suspension systems, despite being a simple 2-degree-of-freedom idea. Researching such a representational model is crucial as a result. The following expressions can be derived using Newton's second law:

$$\begin{aligned} m_s(t)\ddot{w}_s(t) &= -c_s\left[\dot{w}_S(t)-\dot{w}_u(t)\right]-k_s\left[w_s(t)-w_u(t)\right]+u(t) \\ m_u(t)\ddot{w}_u(t) &= c_s\left[\dot{w}_s(t)-\dot{w}_u(t)\right]+k_s\left[w_s(t)-w_u(t)\right]-u(t)-c_u\left[\dot{w}_u(t)-\dot{w}_r(t)\right]-k_u\left[w_u(t)-w_r(t)\right] \end{aligned} \tag{1}$$

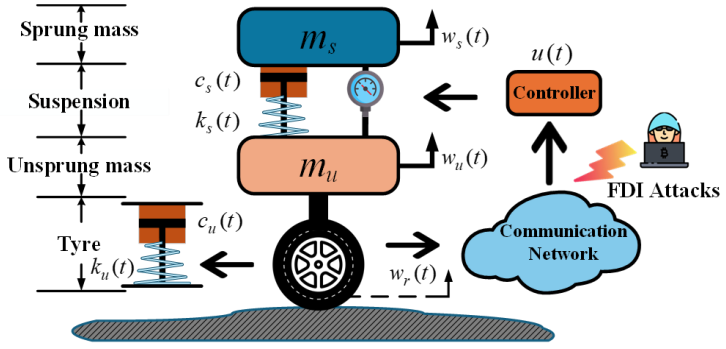

Fig. 1. Quarter-vehicle suspension model

Define the following state variables:

$$\begin{aligned} x_1(t) &= w_s(t)-w_u(t), x_2(t)=\dot{w}_s(t), \\ x_3(t) &= w_u(t)-w_r(t), x_4(t)=\dot{w}_u(t), z(t)=\ddot{w}_s(t) \end{aligned} \tag{2}$$

where m_u stands for the unsprung mass and m_s for the sprung mass. The formula for the actuator force is $u(t)$. The damping and stiffness of the suspension system are denoted by c_s and k_s, respectively. The tire's compressibility and damping are indicated by the k_u and c_u values, respectively. The motion of sprung and unsprung masses is denoted by the letters w_s and w_u, respectively. The road motion input is denoted by w_r. It is possible to determine that $v(t)=\dot{w}_r(t)$

using the velocity input for the disruption. In light of the above-mentioned descriptions, the suspension systems are characterized as follows: Describe $x(t)=\begin{bmatrix} x_1^T & x_2^T & x_3^T & x_4^T \end{bmatrix}^T$. Then the suspension systems are described in the following manner in light of the aforementioned descriptions:

$$\begin{cases} \dot{x}(t) = Ax(t) + Bu(t) + B_v(t)v(t) \\ z(t) = Cx(t) + D(t)u(t) \end{cases} \tag{3}$$

where

$$A=\begin{bmatrix} 0 & 1 & 0 & -1 \\ -\frac{k_s(t)}{m_s(t)} & -\frac{c_s(t)}{m_s(t)} & 0 & \frac{c_s(t)}{m_s(t)} \\ 0 & 0 & 0 & 1 \\ \frac{k_s(t)}{m_u(t)} & \frac{c_s(t)}{m_u(t)} & -\frac{k_u(t)}{m_u(t)} & -\frac{c_s(t)+c_u(t)}{m_u(t)} \end{bmatrix}, B=\begin{bmatrix} 0 \\ \frac{1}{m_s(t)} \\ 0 \\ -\frac{1}{m_u(t)} \end{bmatrix}, B_v=\begin{bmatrix} 0 \\ 0 \\ -1 \\ \frac{c_u(t)}{m_u(t)} \end{bmatrix},$$

$$C=\begin{bmatrix} -\frac{k_s(t)}{m_s(t)} & -\frac{c_s(t)}{m_s(t)} & 0 & \frac{c_s(t)}{m_s(t)} \end{bmatrix}, D=\frac{1}{m_s(t)}.$$

To make the control design easier, denote discrete sampling period T_d. Then, we convert the continuous-time model (3) into a discrete-time model using the Euler discretization method $\dot{x}(t) \approx \frac{x(h+1)-x(h)}{T_d}$:

$$\begin{cases} x(h+1) = A^d x(h) + B^d u(h) + B_v^d v(h) \\ z(h) = C^d x(h) + D^d u(h) \end{cases} \tag{4}$$

where $A^d = T_d A + I, B^d = T_d B, B_v^d = T_d B_v, C^d = C, D^d = D$.

The vehicle's sprung mass and unsprung mass will vary as a result of the loading and unloading of body cargo, passenger up-and-down, tire wear, and other factors. Consequently, the suspension system (4) must be modeled as a mass uncertainty model, meaning that m_s and m_u are unknown.

Think about assuming a range for $m_s(t)$ and $m_u(t)$. $m_s(t) \in [m_{smin}, m_{smax}], m_u(t) \in [m_{umin}, m_{umax}]$. Next, define the following variables:

$$\begin{cases} x(h+1) = \sum_{i=1}^{4} \zeta_i(\varsigma(h)) \left[A_i^d x(h) + B_i^d u(h) + B_{vi}^d v(h) \right] \\ z(h) = \sum_{i=1}^{4} \zeta(\varsigma(h)) \left[C_i^d x(h) + D_i^d u(h) \right] \end{cases} \tag{5}$$

where

$$\begin{aligned} \zeta_1(\varsigma(h)) &= M_1(\varsigma_1(h)) \times N_1(\varsigma_2(h)), \\ \zeta_2(\varsigma(h)) &= M_1(\varsigma_1(h)) \times N_2(\varsigma_2(h)), \\ \zeta_3(\varsigma(h)) &= M_2(\varsigma_1(h)) \times N_1(\varsigma_2(h)), \\ \zeta_4(\varsigma(h)) &= M_2(\varsigma_1(h)) \times N_2(\varsigma_2(h)), \end{aligned} \tag{6}$$

And $M_1(\varsigma_1(h)) = \frac{\frac{1}{m_s(h)} - \check{m}_s}{\hat{m}_s - \check{m}_s}, M_2(\varsigma_1(h)) = \frac{\hat{m}_s - \frac{1}{m_s(h)}}{\hat{m}_s - \check{m}_s}, N_1(\varsigma_2(h)) = \frac{\frac{1}{m_u(h)} - \check{m}_u}{\hat{m}_u - \check{m}_u}, N_2(\varsigma_2(h)) = \frac{\hat{m}_u - \frac{1}{m_u(h)}}{\hat{m}_u - \check{m}_u},$

$\hat{m}_s = max\frac{1}{m_s(h)} = \frac{1}{m_{smin}}, \check{m}_s = min\frac{1}{m_s(h)} = \frac{1}{m_{smax}}, \hat{m}_u = max\frac{1}{m_u(h)} = \frac{1}{m_{umin}}, \check{m}_u = min\frac{1}{m_u(h)} = \frac{1}{m_{umax}}$. $\zeta_i(\varsigma(h))$ is the normalized membership satisfying $\zeta_i(\varsigma(h)) \geq 0$ and $\sum_{i=1}^{4}\zeta(\varsigma(h)) = 1$.

To render a more universally applicable discrete-time T-S fuzzy system, it is formulated with the *i*-th rule as follows in terms of fuzzy dynamics:

Plant Rule *i*: **IF** $\varsigma_1(h)$ is $X_1^i, \varsigma_2(h)$ is $X_2^i, \cdots, \varsigma_n(h)$ is X_n^i, **THEN**

$$\begin{cases} x(h+1) = A_{\zeta(h)}x(h) + B_{\zeta(h)}u(h) + B_{\zeta\nu(h)}\nu(h) \\ z(h) = C_{\zeta(h)}x(h) + D_{\zeta(h)}u(h) \end{cases} \tag{7}$$

The expression $\varsigma_e(x(h))$ represents the premise variables for $e \in \{1,2,\cdots,n\}$ and $i \in \{1,2,\cdots,m\}$. X_n^i denotes the fuzzy associated with rule *i*. The normalized membership function $\zeta_i(\varsigma(h))$ satisfies $\zeta_i(\varsigma(h)) \geq 0$ and $\sum_{i=1}^{m}\zeta_i(\varsigma(h)) = 1$. And

$$A_{\zeta(h)} = \sum_{i=1}^{m}\zeta_i(\varsigma(h))A_i^d, B_{\zeta(h)} = \sum_{i=1}^{m}\zeta_i(\varsigma(h))B_i^d, B_{\zeta\nu(h)} = \sum_{i=1}^{m}\zeta_i(\varsigma(h))B_{vi}^d,$$
$$C_{\zeta(h)} = \sum_{i=1}^{m}\zeta_i(\varsigma(h))C_i^d, D_{\zeta(h)} = \sum_{i=1}^{m}\zeta_i(\varsigma(h))D_i^d$$

2.2. Description of FDI Attack and Controller Design

Due to the open communication environment of NCSs, FDI attacks can take over physical devices or network nodes, introduce inaccurate or meaningless data into the system, disrupt the flow of control signals from sensors to controllers, and alter measurement outcomes. However, it is extremely difficult for the attacker to totally alter the control signal in real-world applications because of the attacker's limited energy. First, the random activation behavior of FDI attacks is represented by the Bernoulli variable $\chi(h)$ with equal probability, taking into account the randomness of FDI attacks. The attacked signal is then assumed to be defined as follows:

$$\tilde{x}(h) = \chi(h)(f_x(h) - x(h)) + x(h) \tag{8}$$

which has the following characteristics：

$$\Pr ob\{\chi(h) = 1\} = \bar{\chi}, \Pr ob\{\chi(h) = 0\} = 1 - \bar{\chi}, \mathrm{E}\{\chi(h)\} = \bar{\chi}, \mathrm{E}\left\{(\chi(h) - \bar{\chi})^2\right\} = \bar{\chi}(1 - \bar{\chi}) = \rho_\chi^2.$$

where $\bar{\chi}$ and ρ_χ^2 stand for the arithmetic variance and expectation of $\chi(h)$, respectively. $f_\chi(h)$ is represented by the cyberspace assault signal, and its energy constraint is as follows:

Assumption 1: The energy signal $f_\chi(h)$ meets the following inequality by giving a matrix Y_1:

$$\| f_\chi(h) \|_2 \leq \| \mathrm{Y}_1 x(h) \|_2 \tag{9}$$

When $\chi(h) = 1$ indicated the presence of an attack in the real network environment. When $\chi(h) = 0$, the system is absent to deception attacks.

Different from the traditional parallel distributed compensation (PDC) method, this paper establishes the following non-PDC controller:

$$u(h) = Q_{\zeta(h)}S_{\zeta(h)}^{-1}\tilde{x}(h) \tag{10}$$

where $Q_{\zeta(h)} \in \square^{n_u \times n_x}, S_{\zeta(h)} \in \square^{n_x \times n_x}$ ⋱ . Which $Q_{\zeta(h)}$ and $S_{\zeta(h)}$ will be solved in the following theorem. Equations (7), (8), and (10) together with the FDI attack signal's probability expectation, allow us to get

$$\begin{cases} x(h+1)=\left(A_{\zeta(h)}+(1-\bar{\chi})\Delta_1\right)x(h)+\left(\chi(h)-\bar{\chi}\right)\Delta_1\left(-x(h)+f_\chi(h)\right)+\bar{\chi}\Delta_1 f_\chi(h)+B_{\zeta\nu(h)}\nu(h) \\ z(h)=\left(C_{\zeta(h)}+(1-\bar{\chi})\Delta_2\right)x(h)+\left(\chi(h)-\bar{\chi}\right)\Delta_2\left(-x(h)+f_\chi(h)\right)+\bar{\chi}\Delta_2 f_\chi(h) \end{cases} \tag{11}$$

where $\Delta_1 = B_{\zeta(h)}Q_{\zeta(h)}S_{\zeta(h)}^{-1}, \Delta_2 = D_{\zeta(h)}Q_{\zeta(h)}S_{\zeta(h)}^{-1}$.

3. Exponential Stability Condition

Lemma 1 [13]: Given a positive definite symmetric matrix $P>0$, if there exists a matrix G such that the following inequality is satisfied:

$$-G^T P^{-1} G \le P\ -G^T - G \tag{12}$$

Theorem 1: Given the positive scalar $\rho_\chi > 0$, attenuation coefficient $\beta > 1$. Controller gain matrices $Q_{\zeta(h)}, S_{\zeta(h)}$. Then the system guaranteeing $H\infty$ performance is exponentially stable under FDI attacks if there exists a positive symmetric matrix $P_{\zeta(h)} > 0$ such that

$$\Phi_{\zeta\chi} = \begin{bmatrix} \Phi_{\zeta\chi}^{11} & * & * & * & * & * \\ M_1 & -P_{\zeta(h+1)} & * & * & * & * \\ \rho_\chi M_2 & 0 & -P_{\zeta(h+1)} & * & * & * \\ M_3 & 0 & 0 & -I & * & * \\ \rho_\chi M_4 & 0 & 0 & 0 & -I & * \\ M_5 & 0 & 0 & 0 & 0 & -P_{\zeta(h)} \end{bmatrix} < 0 \tag{13}$$

where

$$\Phi_{\zeta\chi}^{11} = \begin{bmatrix} -P_{\zeta(h)}^{-1} & * & * \\ 0 & -\theta P_{\zeta(h)}^{-1} & * \\ 0 & 0 & -\gamma^2 I \end{bmatrix}, M_1 = \begin{bmatrix} \beta\left(A_{\zeta(h)}+(1-\bar{\chi})\Delta_1\right) & \beta\bar{\chi}\Delta_1 & \beta B_{\zeta\nu(h)} \end{bmatrix}, M_2 = \begin{bmatrix} -\beta\Delta_1 & \beta\Delta_1 & 0 \end{bmatrix},$$

$$M_3 = \begin{bmatrix} C_{\zeta(h)}+(1-\bar{\chi})\Delta_2 & \bar{\chi}\Delta_2 & 0 \end{bmatrix}, M_4 = \begin{bmatrix} -\Delta_2 & \Delta_2 & 0 \end{bmatrix}, M_5 = \begin{bmatrix} \sqrt{\theta}\mathrm{Y}_1 & 0 & 0 \end{bmatrix}.$$

Proof: Taking into account the deception attacks' energy function constraint (9) with a matrix $P_{\zeta(h)}^{-1}$, we can acquire

$$\theta x^T(h)\mathrm{Y}_1^T P_{\zeta(h)}^{-1}\mathrm{Y}_1 x(h) - \theta f_\chi^T(h) P_{\zeta(h)}^{-1} f_\chi(h) \ge 0 \tag{14}$$

The following candidate function for the Lyapunov function is chosen using the homogeneous polynomial approach after taking into account the influence of the membership function in this work:

$$V\left(x(h),\zeta\right) = \beta^{2h} x^T(h) P_{\zeta(h)}^{-1} x(h) \tag{15}$$

By defining the difference $\Delta V\left(x(h),\zeta\right) = V\left(x(h+1),\zeta\right) - V\left(x(h),\zeta\right),$ using the forward difference, we can obtain

$$\mathrm{E}\left\{\Delta V\left(x(h),\zeta\right)\right\} = \mathrm{E}\left\{\beta^{2(h+1)} x^T(h+1) P_{\zeta(h+1)}^{-1} x(h+1) - \beta^{2h} x^T(h) P_{\zeta(h)}^{-1} x(h)\right\} \tag{16}$$

Denote $\eta(h) = \begin{bmatrix} x^T(h) & f_\chi^T(h) & \nu^T(h) \end{bmatrix}^T$ as the augmented state vector in accordance with (16), and the following formulas also hold:

$$\mathrm{E}\left\{\Delta V\left(x(h),\zeta\right)\right\} = \beta^{2h} * \mathrm{E}\left\{\eta^T(h)\left(M_1^T P_{\zeta(h+1)}^{-1} M_1 + \rho_\chi^2 M_2^T P_{\zeta(h+1)}^{-1} M_2\right)\eta(h) - x^T(h) P_{\zeta(h)}^{-1} x(h)\right\} \tag{17}$$

where $M_1 = \left[\beta\left(A_{\zeta(h)} + (1-\bar{\chi})\Delta_1 \right) \quad \beta\bar{\chi}\Delta_1 \quad \beta B_{\zeta s(h)} \right], M_2 = \left[-\beta\Delta_1 \quad \beta\Delta_1 \quad 0 \right].$

Then, taking into account the known closed-loop system (11) and condition (13), if $\Phi_{\zeta\chi} < 0$ and since $\beta^{2h} > 0$, we will be able to determine that

$$\begin{aligned} &\mathrm{E}\left\{ \Delta V\left(x(h),\zeta\right) + \beta^{2h}\left(z^T(h)z(h) - \gamma^2 s^T(h)s(h) \right) + \theta x^T(h)\mathrm{Y}_1^T P_{\zeta(h)}^{-1}\mathrm{Y}_1 x(h) - \theta f_\chi^T(h) P_{\zeta(h)}^{-1} f_\chi(h) \right\} \\ &= \beta^{2h}\eta^T(h)\left(\Phi_{\zeta\chi}^{11} + M_1^T P_{\zeta(h+1)}^{-1} M_1 + \rho_\chi^2 M_2^T P_{\zeta(h+1)}^{-1} M_2 + M_3^T M_3 + \rho_\chi^2 M_4^T M_4 + M_5^T P_{\zeta(h)}^{-1} M_5 \right)\eta(h) \\ &= \beta^{2h}\eta^T(h)\Phi_{\zeta\chi}\eta(h) \le 0 \end{aligned} \tag{18}$$

Since $z^T(h)z(h) > 0$ when $s(h) = 0$, it may be inferred from (18) that

$$\beta^2 V\left(x(h+1),\zeta\right) - V\left(x(h),\zeta\right) < 0 \tag{19}$$

It goes without saying that $\beta^2 V\left(x(h+1),\zeta\right) < V\left(x(h),\zeta\right)$, thus we can further promote that

$$V\left(x(h),\zeta\right) < \beta^{-2}V\left(x(h-1),\zeta\right) < \beta^{-4}V\left(x(h-2),\zeta\right) < \cdots < \beta^{-2n}V\left(x(h-n),\zeta\right) < \cdots < \beta^{-2h}V(0) \tag{20}$$

Next, it is obtainable from (20) that

$$\xi_1 \| x(h) \|^2 < V\left(x(h),\zeta\right) < \beta^{-2h}\xi_2 \| x(0) \|^2 \tag{21}$$

where $\xi_1 = \left(\lambda_{max}\left(P_{\zeta(h)} \right) \right)^{-1}, \xi_2 = \left(\lambda_{min}\left(P_{\zeta(h)} \right) \right)^{-1}$, which suggests that

$$\| x(h) \| < \sqrt{\frac{\xi_2}{\xi_1}}\beta^{-h} \| x(0) \| \tag{22}$$

and the system (11) is exponentially stable.

By summing the two sides of the equation (18) from 0 to ∞ inside the zero-initial condition, and because $V\left(x(\infty),\zeta\right) \ge 0$ in the presence of an external disturbance $\nu(h) \ne 0$, we can obtain that

$$\mathrm{E}\left\{ \sum_{h=0}^{\infty} z^T(h)z(h) \right\} \le \gamma^2 \sum_{h=0}^{\infty} \nu^T(h)\nu(h) \tag{23}$$

whereby the proof is finished and the $H\infty$ performance index is satisfied.

It should be noted that due to certain nonlinear elements in (13), it is difficult to determine the controller gains. To address the problem, after defining the matrix $\mathrm{Y} = diag\{S_{\zeta(h)}^T, S_{\zeta(h)}^T, I, I, I, I, I, I\}$, an inequality for ensuring (13) can be obtained by pre- and post-multiplying (13) by Y and Y^T:

$$\bar{\Phi}_{\zeta\chi} = \begin{bmatrix} \Omega_1 & * & * & * & * & * & * & * \\ 0 & \theta\Omega_1 & * & * & * & * & * & * \\ 0 & 0 & -\gamma^2 I & * & * & * & * & * \\ \Omega_2 & \Omega_7 & \Omega_{11} & -P_{\zeta(h+1)} & * & * & * & * \\ \Omega_3 & \Omega_8 & 0 & 0 & -P_{\zeta(h+1)} & * & * & * \\ \Omega_4 & \Omega_9 & 0 & 0 & 0 & -I & * & * \\ \Omega_5 & \Omega_{10} & 0 & 0 & 0 & 0 & -I & * \\ \Omega_6 & 0 & 0 & 0 & 0 & 0 & 0 & -P_{\zeta(h)} \end{bmatrix} \tag{24}$$

where

$$\Omega_1 = P_{\zeta(h)} - S_{\zeta(h)} - S_{\zeta(h)}^T, \Omega_2 = \beta A_{\zeta(h)} S_{\zeta(h)} + \beta(1-\bar{\chi}) B_{\zeta(h)} Q_{\zeta(h)}, \Omega_3 = -\rho_\chi \beta B_{\zeta(h)} Q_{\zeta(h)},$$

$$\Omega_4 = C_{\zeta(h)} S_{\zeta(h)} + (1-\bar{\chi}) D_{\zeta(h)} Q_{\zeta(h)}, \Omega_5 = -\rho_\chi D_{\zeta(h)} Q_{\zeta(h)}, \Omega_6 = \sqrt{\theta} \mathrm{Y} S_{\zeta(h)}, \Omega_7 = \beta \bar{\chi} B_{\zeta(h)} Q_{\zeta(h)},$$

$$\Omega_8 = \rho_\chi \beta B_{\zeta(h)} Q_{\zeta(h)}, \Omega_9 = \bar{\chi} D_{\zeta(h)} Q_{\zeta(h)}, \Omega_{10} = \rho_\chi D_{\zeta(h)} Q_{\zeta(h)}, \Omega_{11} = \beta B_{\zeta\nu(h)}.$$

4. Simulation Results

Setting $T_d = 0.001[s]$, $\beta = 1.0025$, Table I [14] displays the pertinent active suspension characteristics. This study examines a particular example in which m_u stays constant but m_s fluctuates. The controller gain matrices are then computed using Theorem 1's requirement of exponential stability of the system:

Table 1 Parameters of active suspension model.

Parameters	Value	Parameters	Value
k_s	900 [N/m]	k_u	2500 [N/m]
m_s	[2.45,2.9] [kg]	m_u	1 [kg]
c_s	7.5 [N · s/m]	c_u	5 [N · s/m]
z_{max}	0.038 [m]	u_{max}	38.3 [N]

$$Q_1 = \begin{bmatrix} 10^{-4} \times 3.6630 & -0.0049 & -10^{-5} \times 9.5034 & 0.0039 \end{bmatrix}, Q_2 = \begin{bmatrix} 10^{-4} \times 3.6995 & -0.0053 & -10^{-5} \times 9.6893 & 0.0054 \end{bmatrix}$$

$$S_1 = 10^{-4} \times \begin{bmatrix} 0.00432 & -0.0337 & -0.0012 & 0.0025 \\ -0.0337 & 0.4907 & 0.0081 & -0.15356 \\ -0.0011 & 0.0081 & 0.0012 & -0.0103 \\ 0.0025 & -0.1530 & -0.0103 & 2.9955 \end{bmatrix}, S_2 = 10^{-4} \times \begin{bmatrix} 0.0043 & -0.0338 & -0.0012 & 0.0025 \\ -0.0338 & 0.4918 & -0.0081 & -0.1579 \\ -0.0012 & 0.0081 & -0.0012 & -0.1027 \\ 0.0025 & -0.1591 & -0.1028 & 3.0272 \end{bmatrix}$$

The road displacement input is defined as:

$$\mathrm{z}_r(h) = \begin{cases} 0.02 & h \in [0.1+nF, 1.6+nF] \\ 0 & h \notin [0.1+nF, 1.6+nF] \end{cases} \tag{25}$$

where $n \in \{0,1,2,3\}$ and $F = 3[s]$. The simulation test using Simulink yields the following primary comparative results based on the aforementioned parameter values and the pertinent control gain matrices.

The main results of the suspension system under three working conditions are shown in Fig. 2-Fig. 4, that is, passive suspension, FDI attacks suffered, and the control method of no attack. Fig. 2 (a) is the state response of the suspension system. When excited by a pulse road surface, the passive suspension cannot return to a stable state. In the event of FDI attacks, the system's state can eventually be restored to stability due to the controller's role. Without any attack, the state only changes upon encountering a pulse and can quickly stabilize. As illustrated in Fig. 2(b), in the absence of control, the tire and body under the passive suspension continuously jitter when encountering a road pulse. However, with the controller designed in this study, both the tire and body can respond to impulse interference and rapidly regain stability. Fig. 3 (a) and Fig. 3 (b) display the actuator force and sprung mass acceleration under various operating situations, showing that the controller developed in this research may lower the suspension's vertical acceleration while still meeting the actuator torque limitation $|u(t)| \leq 38.3N$. A more comfortable driving experience will result from simultaneous improvements to the suspension system's dynamic deflection and relative dynamic tire load.

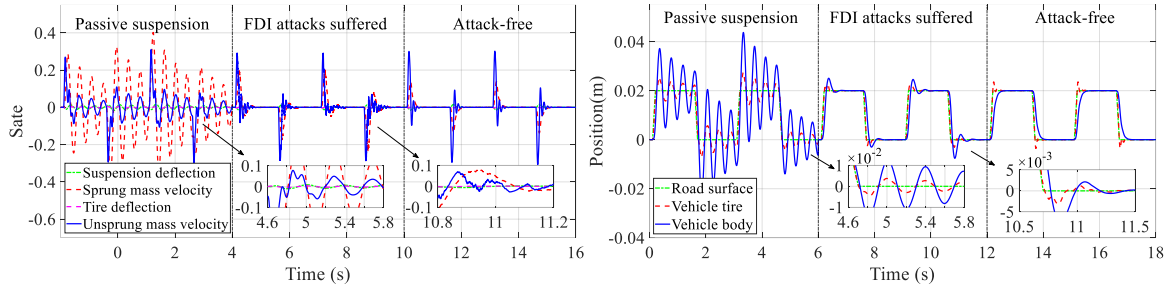

(a) (b)

Fig. 2. (a) State response curve of suspension system under impulse road excitation. (b) The displacement change of each stroke in the vertical direction under the excitation of pulse road surface.

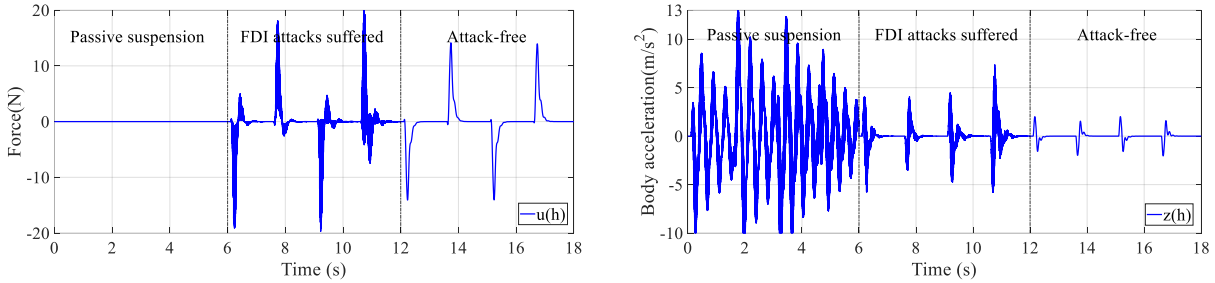

(a) (b)

Fig. 3. (a) Actuator force under different conditions. (b) Sprung mass acceleration under different conditions.

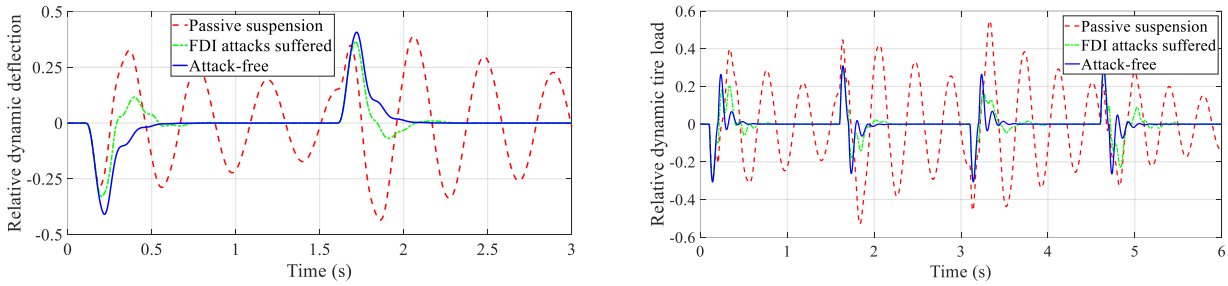

(a) (b)

Fig. 4. (a) Relative dynamic deflection. (b) Relative dynamic tire load.

The relative dynamic deflection $(w_s - w_u)/w_{max}$ and relative dynamic load $k_u(w_u - w_r)/(m_s + m_u)g$ of the suspension system with or without control are displayed in Table II and Fig. 4. Even though the acceleration of the sprung mass is the primary focus of this research from the standpoint of performance limitations, it is possible to confirm through simulation that it fulfills $(w_s - w_u)/w_{max} < 1$ and $k_u(w_u - w_r)/(m_s + m_u)g < 1$ without taking these two hardware constraints into account. The vehicle body's vertical acceleration, relative dynamic disturbance, and relative dynamic load are all reduced by 89.5%, 49.41%, and 69.84% on the RMS index, respectively, in comparison to the passive suspension. This further confirms that the approach proposed in this paper can improve riding comfort.

Table 2 RMS performance index values for the rough road profile.

Method	$\ddot{w}_s$	$\frac{w_s - w_u}{w_{max}}$	$\frac{k_u(w_u - w_r)}{(m_s + m_u)g}$
Passive suspension	4.4971	0.1943	0.2195
Control strategy in this paper	0.4724 (-89.5%)	0.0983 (-49.41%)	0.0662 (-69.84%)

5. Conclusions

Through rigorous theoretical analysis and simulation validation, the control strategy proposed in this study demonstrates the exponential stability of the system. Additionally, this strategy ensures the vehicle's stability and security under covert FDI attacks. According to the results, the suspension system with a resilient controller performs better. More complex external conditions should be taken into account in future studies, and controllers that can balance harsh limitations like dynamic loads on the suspension system and dynamic disturbances with driving comfort should be developed.

References

[1] Sun W, Pan H, Gao H. Filter-based adaptive vibration control for active vehicle suspensions with electrohydraulic actuators[J]. IEEE Transactions on Vehicular Technology, 2015, 65(6): 4619-4626.

[2] Huang W, Zhao J, Yu G, et al. Intelligent vibration control for semiactive suspension systems without prior knowledge of dynamical nonlinear damper behaviors based on improved extreme learning machine[J]. IEEE/ASME Transactions on Mechatronics, 2020, 26(4): 2071-2079.

[3] Bégin M A, Chouinard P, Lebel L P, et al. Experimental assessment of a controlled slippage magnetorheological actuator for active seat suspensions[J]. IEEE/ASME Transactions on Mechatronics, 2018, 23(4): 1800-1810.

[4] Liu Y J, Zhang Y Q, Liu L, et al. Adaptive finite-time control for half-vehicle active suspension systems with uncertain dynamics[J]. IEEE/ASME Transactions on Mechatronics, 2020, 26(1): 168-178.

[5] Fei Z, Wang X, Liu M, et al. Reliable control for vehicle active suspension systems under event-triggered scheme with frequency range limitation[J]. IEEE Transactions on Systems, Man, and Cybernetics: Systems, 2019, 51(3): 1630-1641.

[6] Zhang Z, Li H, Wu C, et al. Finite frequency fuzzy $H\infty$ control for uncertain active suspension systems with sensor failure[J]. IEEE/CAA Journal of Automatica Sinica, 2018, 5(4): 777-786.

[7] Wang R, Jing H, Wang J, et al. Robust output-feedback based vehicle lateral motion control considering network-induced delay and tire force saturation[J]. Neurocomputing, 2016, 214: 409-419.

[8] Li W, Xie Z, Zhao J, et al. Static-output-feedback based robust fuzzy wheelbase preview control for uncertain active suspensions with time delay and finite frequency constraint[J]. IEEE/CAA Journal of Automatica Sinica, 2020, 8(3): 664-678.

[9] Guo J, Wang J, Luo Y, et al. Takagi–Sugeno fuzzy-based robust $H\infty$ integrated lane-keeping and direct yaw moment controller of unmanned electric vehicles[J]. IEEE/ASME Transactions on Mechatronics, 2020, 26(4): 2151-2162.

[10] Shan Y, Xie X, Peng C. Resilient Stabilization of Networked Active Suspension Systems via a Multi-Instantaneous Fuzzy Gain-Scheduling Mechanism[J]. IEEE Transactions on Industrial Informatics, 2024. doi: 10.1109/TMECH.2024.3476245.

[11] Liang J, Feng J, Lu Y, et al. A direct yaw moment control framework through robust TS fuzzy approach considering vehicle stability margin[J]. IEEE/ASME Transactions on Mechatronics, 2023, 29(1): 166-178.

[12] Hussain F, Hussain R, Hassan S A, et al. Machine learning in IoT security: Current solutions and future challenges[J]. IEEE Communications Surveys & Tutorials, 2020, 22(3): 1686-1721.

[13] Shan Y, Xie X P, Mao Z. Co-Design of a Switching-Type Control Scheme for Nonlinear Networked Systems With Protocol-Based Communication and Its Application to Circuits[J]. IEEE Transactions on Automation Science and Engineering, 2024. doi: 10.1109/TMECH.2024.3476245.

[14] Shan Y, Xie X, Sun J, et al. Resilient Design of Networked Security Control for Active Suspension Systems via an Augmented Switching-Type Approach[J]. IEEE/ASME Transactions on Mechatronics, 2024. doi: 10.1109/TMECH.2024.3476245.